SCIEPublish

Article

WO_3 Photoanodes for Photoelectrochemical Applications

Barbora Radová [1], Tomáš Imrich [1], Hana Krýsová [2], Michael Neumann-Spallart [1] and Josef Krýsa [1,*]

[1] Department of Inorganic Technology, University of Chemistry and Technology Prague, Technická 5, 166 28 Prague, Czech Republic; radovar@vscht.cz (B.R.); imricht@vscht.cz (T.I.); neumannspallart@gmail.com (M.N.-S.)

[2] J. Heyrovský Institute of Physical Chemistry of the Czech Academy of Sciences, Dolejškova 2155/3, 182 23 Prague, Czech Republic; hana.krysova@jh-inst.cas.cz (H.K.)

* Corresponding author. E-mail: josef.krysa@vscht.cz (J.K.)

Received: 7 January 2025; Accepted: 27 February 2025; Available online: 7 March 2025

ABSTRACT: WO_3 layers were prepared by spray pyrolysis of a peroxotungstic acid solution on FTO/glass substrates. Investigated parameters were layer thickness and influence of post-annealing in air. Films deposited at 250 °C were amorphous. Post-annealing at 550 °C for 2 h resulted in the formation of monoclinic crystalline structure. A comprehensive account of electrochemical efficiency in terms of IPCE for WO_3 films as a function of the three parameters (wavelength, thickness and direction of light incidence) fully characterizing the photoelectrodes is presented here for the first time. The highest improvement in crystallinity and also the highest photocurrent response was found for WO_3 layers deposited at 250 °C and post-annealed at 550 °C, namely 1.9 mA/cm^2 (in 0.1 M $HClO_4$ at 1.6 V *vs.* Ag/AgCl) under irradiation with a solar simulator (AM 1.5, 100 mW/cm^2) and IPCE = 0.5 at 369 nm (front side irradiation), which is comparable with values obtained by other deposition techniques (e.g., hydrothermal or sol gel). Spray pyrolysis as a method of fabricating WO_3 electrodes has the advantage of being able to produce large electrodes for use in practical applications.

Keywords: WO_3; Spray pyrolysis; Crystallinity; Photocurrent; IPCE

1. Introduction

Metal oxide semiconductor materials are attractive for light absorbers, gas sensors, and as catalysts in photoelectrochemical (PEC) processes with applications in (i) light-assisted water electrolysis [1–3], (ii) degradation (oxidation) of organic substances [4–6] and (iii) photoelectrochemical syntheses of chemicals (e.g., I_2, Br_2 or Cl_2) [7]. Much attention has been paid to photoanodes made of binary transition n-type metal oxide materials such as TiO_2 or WO_3. TiO_2 has a wide bandgap of 3.2 eV, which limits its use (λ_{onset} = 388 nm). Less than 4% of the incident power (1.5% of all photons) of the solar light, based on published AM1.5 solar spectra (G-173), can be used by TiO_2 [8]. On the other hand, tungsten trioxide is an n-type semiconducting metal oxide, which has a lower bandgap, *i.e.*, 2.7 eV [9], allowing the utilization of a more substantial portion of the solar light spectrum (λ_{onset} = 459 nm), *i.e.*, approximately 12% of the power (6.2% of all photons) [8].

Dissolution of WO_3 in alkaline media (pH > 6) [10] limits its working range. A possible way of extending it is to cap the WO_3 electrode with a thin protective TiO_2 overlayer. A 20 nm thick TiO_2 layer fabricated by atomic layer deposition on WO_3 decreased the Faradaic efficiency of photocorrosion about 20 times [11].

WO_3 films have been synthesized in many different ways: doctor blading [12], brush painting [13,14], drop casting [5], chemical bath deposition and hydrothermal synthesis [15–18], spin coating [19], sol gel [20], printing [21,22], thermal evaporation [23], sputtering and High Power Impulse Magnetron Sputtering (HiPIMS) [24–26], pulsed laser deposition (PLD) [27], electrodeposition [28,29], anodization [30,31], spray and aerosol pyrolysis [1,32–35], and electrospray deposition [36]. Spray pyrolysis as a method of fabricating WO_3 electrodes has the advantage of being able to produce large electrodes for use in practical applications in contrary to aerosol pyrolysis where the homogeneous distribution of aerosol on larger area is quite challenging.

https://doi.org/10.70322/prp.2025.10006

Crucial parameters influencing the photocurrent of WO_3 films are layer thickness and direction of the incident light (through the electrolyte "EE", or through the substrate "SE" (if transparent, e.g., FTO/glass)) and should be optimized according to the intended usage. For monochromatic irradiation (365 nm) a layer thickness of around 1 µm was found sufficient to achieve maximum photoresponse, and the reported incident photon to current efficiency (IPCE) value for an applied potential of 1.2 V *vs.* SCE was 0.45 [13]. The IPCE for the whole wavelength range was measured for a 1 µm thick WO_3 film and was found to correlate well with light absorptance [13]. The integral of the product of IPCE and the solar flux gave the total expected solar photocurrents using the respective electrodes: 0.79 mA/cm^2 under backside illumination. Recently, using a solar simulator (AM1.5 (1 sun)) and a potential of 0.9 V *vs.* Ag/AgCl in 0.1 M $HClO_4$, a photocurrent density around 1 mA/cm^2 was achieved for a 4 micron thick film obtained by aerosol pyrolysis [1].

In the literature, photocurrents are often reported for various light sources, but comparison with literature data is possible only when wavelength and irradiance are reported or when standardised solar illumination (1.5 AM, 100 mW/cm^2) is used or the whole IPCE spectrum is given.

This study aimed to synthesize mechanically stable WO_3 films by spray pyrolysis with high photocurrent values in aqueous solution under (simulated) solar AM1.5 front side irradiation by optimizing layer thickness. Besides the use of standardised solar illumination (1.5 AM, 100 mW/cm^2) IPCE measurements from both electrolyte/electrode (EE) and substrate/electrode (SE) directions were performed. Such optimized films can be used for photoelectrochemical degradation of water pollutants and/or photoelectrosynthesis of chemicals.

2. Experimental

The chemicals used as received in this work included tungstic acid 99% (Sigma-Aldrich, Burlington, MA, USA), hydrogen peroxide (≥30.0%, Lach-ner, Czech Republic), and perchloric acid (70%, Acros Organics, Geel, Belgium). Triple distilled water was used for the preparation of solutions. Fluorine-doped tin oxide coated 2 mm thick glass ("FTO", 7 Ω/sq., Sigma-Aldrich), was used as a substrate. Substrates were pre-cleaned ultrasonically by degreasing with trichloroethylene followed by rinsing with acetone, ethanol and water and drying in a stream of argon. WO_3 films were deposited from a solution of peroxotungstic acid prepared by suspending tungstic acid powder in 15 vol.% hydrogen peroxide as described previously in [32]. After stirring for 72 h, a slightly yellowish clear solution was obtained. This solution was further diluted to the concentration of 37.5 mM. Details of the spray pyrolysis (SP) apparatus have been described previously [37,38].

The structural, morphological and optical properties of the deposited WO_3 films were determined by X-ray diffraction (X'pert Philips MPD with a Panalytical X'celerator detector using graphite monochromatized Cu-K_α radiation (wavelength 1.54056 Å)) and profilometric thickness measurements (Dektak XT, Bruker, Billerica, MA, USA). The morphology of the films was also characterized by atomic force microscopy (AFM, Dimension Icon, Bruker) in semicontact (tapping) mode. A silicon cantilever (VTESPA-300) with a resonant frequency, f_{res}, of approx. 300 kHz, a spring constant, k, of 42 N/m, and a nominal tip radius of 5 nm (Bruker) were employed. The Gwyddion software (v. 2.53) was used for processing AFM image data and for the calculation of the roughness factor (R_f), which represents the ratio between the three-dimensional surface area of the image and its two-dimensional footprint area.

Photoelectrochemical measurements used a Voltalab 10 PGZ-100 potentiostat and an Ag/AgCl reference electrode. Voltammetry was carried out under periodical (5 s light/5 s dark) front side illumination of the electrolyte/electrode interface. An aqueous solution of $HClO_4$ was used as an electrolyte. For irradiation, a solar simulator (150 W Xe arc lamp (Newport) with an AM 1.5G filter, irradiance 1 sun (100 mW/cm^2)) was used. For the quantum efficiency measurements (IPCE) an Electrochemical Photocurrent Spectra CIMPS-pcs system (Zahner, Kronach, Germany) with a TLS03 tunable light source was used.

3. Results and Discussion

WO_3 films were deposited by SP at 250 °C nominal substrate temperature on FTO/glass using a 37.5 mM peroxotungstic acid solution with a spray rate of 1.6 mL/min. The films were annealed in air at 550 °C for 2 h to form the desired monoclinic WO_3 phase.

3.1. Physical Characterization

Spray pyrolysis resulted in well-adherent WO_3 films. Post-annealing at 550 °C had no impact on film adhesion. XRD data of as-deposited WO_3 films and of films after post-annealing at 550 °C are shown in Figure 1. The WO_3 films

deposited at 250 °C did not contain any crystalline phase, only lines corresponding to the FTO/glass substrate were visible. For identification, Raman spectroscopy was therefore carried out and shown in Figure 2. It proved that the deposited layer consisted of amorphous WO_3. Annealing in air at 550 °C for 2 h resulted in the formation of the WO_3 monoclinic crystalline structure.

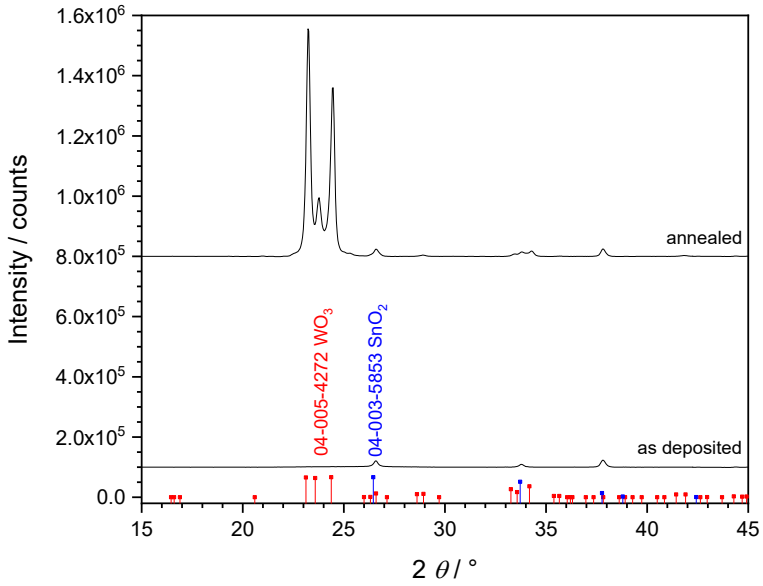

Figure 1. XRD patterns of as-deposited WO_3 films (250 °C) (lower trace) and post-annealed films in air (550 °C, 2 h) (higher trace). The thickness of the WO_3 layers was ~4 µm. XRD reference lines [39]: 04-005-4272 tungsten trioxide (WO_3) and 04-003-5833 cassiterite (SnO_2).

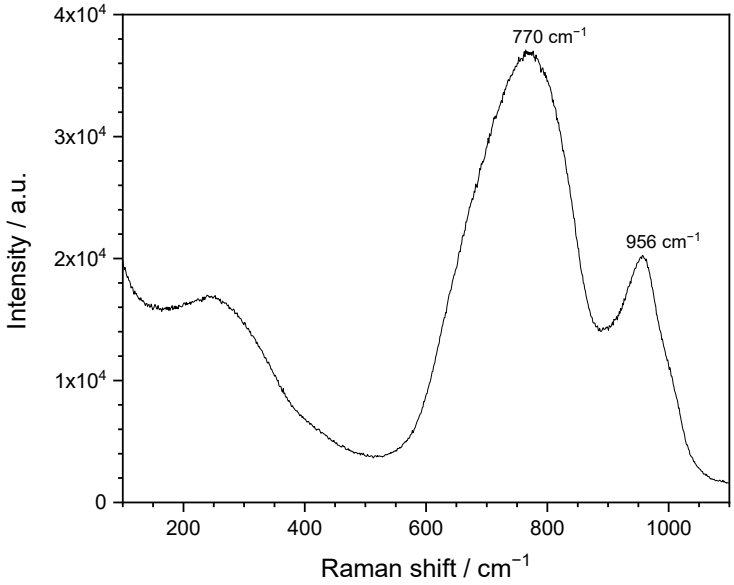

Figure 2. Raman spectrum of an as-deposited (250 °C) WO_3 film. The thickness of the WO_3 layers was 4.2 µm.

Figure S1 (in Supplementary Materials) shows AFM images of the FTO substrate (a) and of a WO_3 film deposited on FTO (250 °C) after post-annealing in air (550 °C, 2 h). The WO_3 film of thickness 4.2 µm was very smooth as seen by the decrease of the roughness factor, R_f, by 20% after coverage of the FTO/glass with a WO_3 layer.

3.2. Photoelectrochemical Characterization

A typical chopped light polarization curve of a WO_3 film deposited at 250 °C WO_3 and post-annealed in air (550 °C, 2 h) is shown in Figure 3. The photocurrent onset was at ~0.25 V *vs.* Ag/AgCl. In the range of potentials from 0.25 to 1.6 V *vs.* Ag/AgCl the dark current was negligible and started to rise at ~1.7 V *vs.* Ag/AgCl. The maximum photocurrent of WO_3 films was achieved at 1.6 V *vs.* Ag/AgCl.

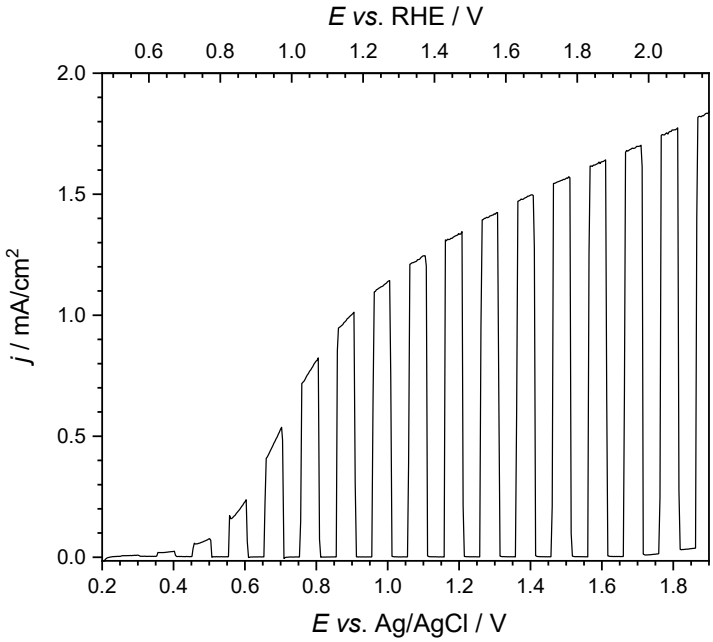

Figure 3. Typical chopped light polarization curve of a WO_3 film deposited at 250 °C WO_3 and post-annealed in air (550 °C, 2 h). Irradiance 1 sun (100 mW/cm^2, simulated AM 1.5G). Electrolyte 0.1 M $HClO_4$ (pH 1).

In the next step, we looked in detail at the influence of layer thickness. Values of IPCE for front side (EE) and back side (SE) illumination of WO_3 films of various thicknesses deposited under these conditions are shown in Figure 4a and 4b, respectively.

(**a**) (**b**)

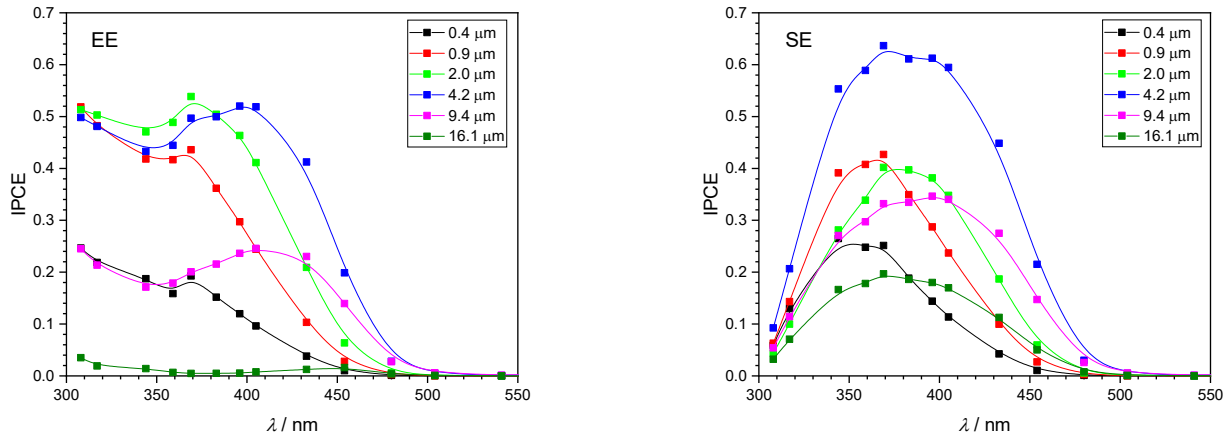

Figure 4. IPCE of WO_3 films deposited at 250 °C WO_3 and post-annealed in air (550 °C, 2 h) of thickness 0.4–16.1 µm. (**a**) front side (EE), (**b**) back side (SE) illumination in 0.1 M $HClO_4$ at 1.6 V *vs.* Ag/AgCl.

A Tauc plot for an indirect electronic transition derived from the IPCE spectrum of a WO_3 film (deposition at 250 °C, post-annealing at 550 °C, layer thickness 4.2 µm) is shown in Figure S2 (in Supplementary Materials). An indirect bandgap of 2.7 eV was determined in accordance with published values [9].

A comprehensive account of electrochemical efficiency in terms of IPCE for WO_3 films as a function of wavelength, thickness and direction of light incidence (EE and SE) is presented here for the first time. Apart from the applied potential (governing the depletion layer width), which was selected to give maximum photocurrents before dark currents started to rise, these three parameters characterize the photoelectrodes fully. A detailed discussion of the dependence of the quantum efficiency on the above-mentioned parameters was given by Popkirov et al. [40].

For thin to medium thick layers, the observed increase in IPCE with thickness was due to the increase of the penetration depth of light, *i.e.*, the IPCE followed the shape of the absorptance spectrum for all thicknesses as described

in [9] and reached a value of 0.5 when all photons were absorbed. Further increase of thickness should keep this value constant but it fell below the optimum. This was probably due to the loss of good electrical contact between grains in the outer layers of the films as often observed in thicker films, impeding the transport of majority carriers towards the back contact (9 and 16 microns for EE irradiation in Figure 4a). An often-used wavelength in practical irradiations is 365 nm as it is a main mercury line, typical for the so called "UVA". At this wavelength, most photons are absorbed within 1 micron. This has already been shown in [13] together with the saturation of IPCE as a function of layer thickness. This result is reproduced in the present study. The decrease of IPCE below 330 nm for SE illumination is due to light absorption by SnO_2 and glass.

It is interesting to note that even the 16 micron thick film which produced only very low IPCE values in the EE mode, produced a maximum IPCE of 0.2 in the SE mode. This can be attributed to a porous film structure. In SE mode, most of the light is absorbed near the back contact so that photogenerated holes can reach the interface to the penetrating electrolyte easily and carry out a charge transfer reaction on the spot. The corresponding conduction band electrons (majority carriers) have to cover only a short distance towards the back contact, in contrast to the difficult transport situation encountered with EE illumination. The example shows again the diagnostic value of conducting EE *vs.* SE illumination experiments. Figure 5 exemplifies the essence of these observations by plotting IPCE at two selected wavelengths and total photocurrent for white light illumination as a function of layer thickness.

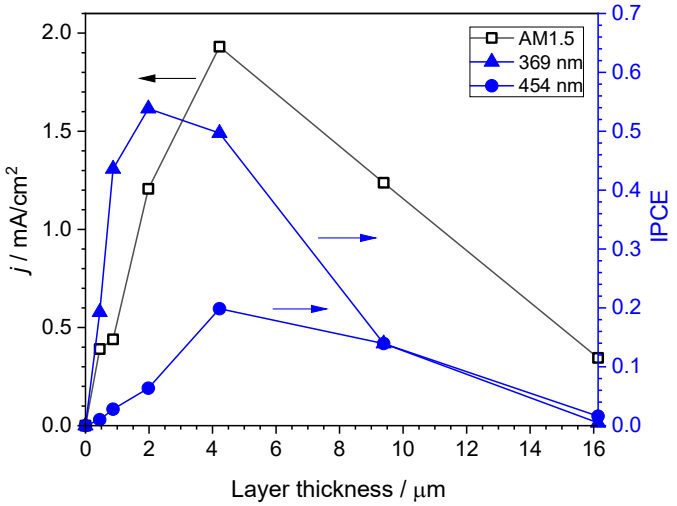

Figure 5. Dependence of photocurrent density and IPCE on layer thickness. Front side simulated solar AM 1.5G irradiation (100 mW/cm^2) (open squares, left *y* axis) and IPCE at 369 nm (filled triangles, right axis) and 454 nm (filled circles, right *y* axis). Electrode potential 1.6 V *vs.* Ag/AgCl, electrolyte 0.1 M $HClO_4$.

Table 1 shows a comparison of photocurrents (1.5 AM solar light) and IPCEs (incident photon to current efficiency) of WO_3 electrodes obtained by various deposition techniques found in the literature together with results obtained in the present study. All films had a monoclinic crystalline structure.

Table 1. Photocurrent densities under AM 1.5 solar irradiation (100 mW/cm^2) and IPCE at 365−369 nm of WO_3 films prepared by various techniques. Front side illumination (through the electrolyte, EE).

Deposition Technique	Layer Thickness/µm	Electrolyte or pH	Photocurrent Density at 1.2 V *vs.* RHE/mA/cm^2	IPCE at 365–369 nm	Ref.
Spray pyrolysis	4.2	0.1 M $HClO_4$	1.1	0.5 (1.6 V *vs.* Ag/AgCl)	this work
Brush painting	1.0–2.7	0.1 M $HClO_4$	-	0.62 (1.2 V *vs.* SCE)	[13]
Hydrothermal	2.3	0.5 M Na_2SO_4	1.6	0.75 (1 V *vs.* SCE)	[18]
Hydrothermal	2.3–3.6	0.9	-	0.53 * (0.95 V *vs.* Ag/AgCl)	[15]
Hydrothermal	3.5	0.1 M $HClO_4$	1.25	0.69 (1.4 V *vs.* Ag/AgCl)	[17]
Sol-gel	1.2	1 M H_2SO_4	2.0	-	[20]
DC-sputtering	0.15	0.1 M Na_2SO_4	0.8	-	[26]
Aerosol pyrolysis	3.8	0.1 M $HClO_4$	1.2	-	[1]
Aerosol pyrolysis	1.5	0.1 M $HClO_4$	-	0.4 (1.3 V *vs.* Ag/AgCl)	[1]
Aerosol pyrolysis	4	0.1 M $HClO_4$	1.05	-	[4]

* at 375 nm.

Reported photocurrent densities for a potential of 1.2 V *vs.* RHE are in the range of 0.8 to 2.0 mA/cm^2. The photocurrent densities achieved in the present work (around 1.1 mA/cm^2) are similar to those fabricated by hydrothermal techniques [17] and slightly higher than that fabricated by aerosol pyrolysis (1.05 mA/cm^2) [1] and DC-sputtering (0.8 mA/cm^2) [26]. The IPCE at 369 nm found in this work was 0.5 for the best electrode. This value is similar to that reported for WO_3 films prepared by aerosol spray pyrolysis using peroxotungstic acid as a precursor (0.4) [1]. Other deposition techniques result in higher values of IPCE. For example, IPCE for a layer-by-layer brush coated electrode using $WOCl_4$ as a precursor [13] was 0.6 and for a hydrothermally grown WO_3 electrode, IPCE values 0.75 [18] and 0.53 [15] was reported. Although WO_3 films prepared by spray pyrolysis (SP) deposition did not achieve the high photocurrent densities and IPCE values as for sol gel or hydrothermal technique, the SP technique is able to fabricate larger WO_3 electrodes needed for practical electrosynthetic, environmentally relevant advanced oxidation processes, and energy conversion applications.

4. Conclusions

As deposited WO_3 layers (temperature 250 °C) were amorphous and the photocurrent density was negligible. Post-annealing at 550 °C resulted in the formation of monoclinic WO_3 and high photocurrent density.

Apart from the applied potential (governing the depletion layer width), which was selected to give maximum photocurrents before dark currents started to rise, parameters as wavelength, thickness and direction of light incidence (EE and SE) characterize the photoelectrodes fully. A comprehensive account of electrochemical efficiency in terms of IPCE for WO_3 films as a function of these three parameters was presented here for the first time.

Optimized WO_3 layers with a thickness of approximately 4 μm, deposited at 250 °C and annealed at 550 °C, exhibited a photocurrent of ~1.9 mA/cm^2 (1.6 V *vs.* Ag/AgCl) and ~1.1 mA/cm^2 (0.9 V *vs.* Ag/AgCl) under irradiation with a solar simulator in 0.1 M $HClO_4$. The IPCE at 369 nm was 0.5 (EE irradiation) for the optimised electrode. In comparison, other deposition techniques as hydrothermal or sol gel technique result in similar values of both photocurrent density and IPCE. On the other hand, spray pyrolysis deposition techniques are able to fabricate larger WO_3 electrodes needed for practical environmental and energy conversion applications.

Supplementary Materials

The following supporting information can be found at: https://www.sciepublish.com/article/pii/445, Figure S1: AFM phase images (left) and 3D height AFM images (right) of (a) FTO/glass substrate, (b) 4.2 μm thick WO_3 layer deposited at 250 °C on FTO/glass substrate and post-annealed at 550 °C for 2 h. The black bar in AFM phase images represents 500 nm; Figure S2: Tauc plot for WO_3 films deposited at 250 °C and post-annealed in air (550 °C, 2 h), layer thickness 4.2 μm.

Acknowledgements

Jiří Olejníček is acknowledged for Raman spectroscopy and Hana Tarábková for AFM analysis.

Author Contributions

B.R.: Investigation, Data curation, T.I.: Investigation, Data curation, Original draft, Writing—review & editing, H.K.: Investigation, M.N.-S.: Conceptualization, Original draft, Writing—review & editing, J.K.: Funding acquisition, Conceptualization, Writing—review & editing.

Ethics Statement

Not applicable.

Informed Consent Statement

Not applicable.

Data Availability Statement

The data presented in this study are available at https://doi.org/10.5281/zenodo.14605450. Data set for "WO_3 photoanodes for photoelectrochemical applications" (Original data) (Zenodo).

Funding

This work was supported by the project "Sensors and Detectors for Future Information Society-SENDISO reg. n. CZ.02.01.01/00/22_008/0004596" by the Programme Johannes Amos Comenius, call "Excellent Research". This work was also supported by the Czech Science Foundation (project number 23-05266S) and by the grant of Specific University Research (UCT Prague)-Grant A2_FCHT_2024_002.

Declaration of Competing Interest

The authors declare that they have no known competing financial interests or personal relationships that could have appeared to influence the work reported in this paper.

References

1. Brada M, Neumann-Spallart M, Krýsa J. Tungsten trioxide film photoanodes prepared by aerosol pyrolysis for photoelectrochemical applications. *Catal. Today* **2023**, *413–415*, 113981. doi:10.1016/j.cattod.2022.113981.
2. Zheng G, Wang J, Liu H, Murugadoss V, Zu G, Che H, et al. Tungsten oxide nanostructures and nanocomposites for photoelectrochemical water splitting. *Nanoscale* **2019**, *11*, 18968–18994. doi:10.1039/C9NR06053A.
3. Wang Y, Tian W, Chen C, Xu W, Li L. Tungsten Trioxide Nanostructures for Photoelectrochemical Water Splitting: Material Engineering and Charge Carrier Dynamic Manipulation. *Adv. Funct. Mater.* **2019**, *29*, 1809036. doi:10.1002/adfm.201809036.
4. Brada M, Rusek J, Imrich T, Neumann-Spallart M, Krýsa J. Photoelectrochemical degradation of selected organic pollutants on tungsten trioxide photoanodes. *J. Photochem. Photobiol. A Chem.* **2024**, *457*, 115883. doi:10.1016/j.jphotochem.2024.115883.
5. Sadale SB, Neumann-Spallart M. Drop-cast tungsten trioxide semiconducting films in Photoelectrocatalysis. *J. Electroanal. Chem.* **2020**, *877*, 114502. doi:10.1016/j.jelechem.2020.114502.
6. Imrich T, Neumann-Spallart M, Krýsa J. Photoelectrochemical degradation of selected organic substances on Fe_2O_3 photoanodes: A comparison with TiO_2. *Photochem. Photobiol. Sci.* **2023**, *22*, 419–426. doi:10.1007/s43630-023-00373-w.
7. Imrich T, Neumann-Spallart M, Krýsa J. Bromine generation on various photoanodes: α-Fe_2O_3, Fe_2TiO_5, WO_3 and TiO_2. *Catal. Today* **2024**, *432*, 114627. doi:10.1016/j.cattod.2024.114627.
8. National Renewable Energy Laboratory. *ASTM1.5 Global (ASTMG173) Solar Spectrum*; South Table Mountain Campus: Golden, CO, USA.
9. Butler MA. Photoelectrolysis and physical properties of the semiconducting electrode WO_3. *J. Appl. Phys.* **1977**, *48*, 1914–1920. doi:10.1063/1.323937.
10. Pourbaix M. *Atlas d'Équilibres Électrochimiques*; Gauthier-Villars: Paris, France, 1963.
11. Imrich T, Brada M, Tarábková H, Krýsová H, Neumann-Spallart M, Krýsa J. Extension of the (photo)electrochemical working range of WO_3 electrodes to pH 8 by ALD coverage with TiO_2. *J. Electrochem. Soc.* **2025**, *submitted*.
12. Le HV, Pham PT, Le LT, Nguyen AD, Tran NQ, Tran PD. Fabrication of tungsten oxide photoanode by doctor blade technique and investigation on its photocatalytic operation mechanism. *Int. J. Hydrogen Energy* **2021**, *46*, 22852–22863. doi:10.1016/j.ijhydene.2021.04.125.
13. Gaikwad NS, Waldner G, Brüger A, Belaidi A, Chaqour SM, Neumann-Spallart M. Photoelectrochemical characterization of semitransparent WO_3 films. *J. Electrochem. Soc.* **2005**, *152*, G411. doi:10.1149/1.2047227.
14. Waldner G, Brüger A, Gaikwad NS, Neumann-Spallart M. WO_3 thin films for photoelectrochemical purification of water. *Chemosphere* **2007**, *67*, 779–784. doi:10.1016/j.chemosphere.2006.10.078.
15. Ade M, Schumacher L, Marschall R. Seed layer formation determines photocurrent response of hydrothermally-grown WO_3 photoanodes. *Sustain. Energy Fuels* **2023**, *7*, 4332–4340. doi:10.1039/D3SE00340G.
16. Najdoski MZ, Todorovski T. A simple method for chemical bath deposition of electrochromic tungsten oxide films. *Mater. Chem. Phys.* **2007**, *104*, 483–487. doi:10.1016/j.matchemphys.2007.03.040.
17. Sayed MH, Gomaa MM, Imrich T, Nebel R, Neumann-Spallart M, Krýsa J, et al. Photoelectrochemical properties of WO_3 films prepared by hydrothermal synthesis. *J. Photochem. Photobiol. A Chem.* **2025**, *in press.*
18. Feng X, Chen Y, Qin Z, Wang M, Guo L. Facile fabrication of sandwich structured WO_3 nanoplate arrays for efficient photoelectrochemical water splitting. *ACS Appl. Mater. Interfaces* **2016**, *8*, 18089–18096. doi:10.1021/acsami.6b04871.
19. Omer S, Ullah MS, Shah SAA, Idrees R, Saeed S. Preparation of additive free tungsten trioxide thin films using spin-coating method for electrochemical applications. *Appl. Nanosci.* **2023**, *13*, 5659–5664. doi:10.1007/s13204-023-02779-5.
20. Jelinska A, Bienkowski K, Jadwiszczak M, Pisarek M, Strawski M, Kurzydlowski D, et al. Enhanced photocatalytic water splitting on very thin WO_3 films activated by high-temperature annealing. *ACS Catal.* **2018**, *8*, 10573–10580. doi:10.1021/acscatal.8b02723.

21. Velasco J, Ateka A, de Larramendi IR, del Campo FJ. Electrochromic screen-printed tungsten trioxide electrodes. *Electrochim. Acta* **2024**, *493*, 144414.
22. Králová M, Másilko J, Smilek J, Martinková E, Březina M, Krouská J, et al. Tungsten trioxide coatings prepared by inkjet printing of a water-based formulation: Structural characteristics and electrophotocatalytic properties. *Catal. Today* **2024**, *430*, 114544.
23. Sung PH, Yen HK, Yang SM, Lu KC. Synthesis and physical characteristics of undoped and potassium-doped cubic tungsten trioxide nanowires through thermal evaporation. *Nanomaterials* **2023**, *13*, 4562.
24. Brunclíková M, Hubička Z, Kment Š, Olejníček J, Čada M, Kšírová P, et al. Semiconducting WO_3 thin films prepared by pulsed reactive magnetron sputtering. *Res. Chem. Intermed.* **2015**, *41*, 9259–9266.
25. Olejníček J, Brunclíková M, Kment Š, Hubička Z, Kmentová H, Kšírová P, et al. WO_3 thin films prepared by sedimentation and plasma sputtering. *Chem. Eng. J.* **2017**, *318*, 281–288.
26. Mohamedkhair AK, Drmosh QA, Qamar M, Yamani ZH. Tuning structural properties of WO_3 thin films for photoelectrocatalytic water oxidation. *Catalysts* **2021**, *11*, 1234.
27. Fàbrega C, Murcia-López S, Monllor-Satoca D, Prades JD, Hernández-Alonso MD, Penelas G, et al. Efficient WO_3 photoanodes fabricated by pulsed laser deposition for photoelectrochemical water splitting with high faradaic efficiency. *Appl. Catal. B Environ.* **2016**, *189*, 133–140.
28. Kwong WL, Qiu H, Nakaruk A, Koshy P, Sorrell CC. Photoelectrochemical properties of WO_3 thin films prepared by electrodeposition. *Energy Procedia* **2013**, *34*, 617–626.
29. Kim YO, Yu SH, Ahn KS, Lee SK, Kang SH. Enhancing the photoresponse of electrodeposited WO_3 film: Structure and thickness effect. *J. Electroanal. Chem.* **2015**, *752*, 25–32.
30. Syrek K, Zaraska L, Zych M, Sulka GD. The effect of anodization conditions on the morphology of porous tungsten oxide layers formed in aqueous solution. *J. Electroanal. Chem.* **2018**, *829*, 106–115.
31. Watcharenwong A, Chanmanee W, De Tacconi NR, Kajitvichyanukul P, Rajeshwar K, et al. Growth of nanoporous tungsten trioxide by anodization of tungsten foil: Influence of process variables on morphology, photoelectrochemical response and visible light decomposition of methylene blue. In Proceedings of the 211th ECS Meeting, Chicago, IL, USA, 6–10 May 2007.
32. Sadale SB, Chaqour SM, Gorochov O, Neumann-Spallart M. Photoelectrochemical and physical properties of tungsten trioxide films obtained by aerosol pyrolysis. *Mater. Res. Bull.* **2008**, *43*, 1472–1479.
33. Bertus LM, Duta A. Synthesis of WO_3 thin films by surfactant-mediated spray pyrolysis. *Ceram. Int.* **2012**, *38*, 2873–2882.
34. Patil PS, Patil PR. Photoelectrochemical characterization of sprayed tungsten oxide thin films. *Sol. Energy Mater. Sol. Cells* **1994**, *33*, 293–300.
35. Hunge YM, Mahadik MA, Moholkar AV, Bhosale CH. Photoelectrocatalytic degradation of oxalic acid using WO_3 and stratified WO_3/TiO_2 photocatalysts under sunlight illumination. *Ultrason. Sonochem.* **2017**, *35*, 233–242.
36. Yoon H, Mali MG, Kim MW, Al-Deyab SS, Yoon SS. Electrostatic spray deposition of transparent tungsten oxide thin-film photoanodes for solar water splitting. *Catal. Today* **2016**, *260*, 89–94.
37. Imrich T, Neumann-Spallart M, Krýsová H, Tarábková H, Nebel R, Krýsa J. Ti doped hematite photoanodes: Protective coverage by titania overlayers. *J. Photochem. Photobiol. A Chem.* **2023**, *445*, 115026.
38. Imrich T, Krýsová H, Neumann-Spallart M, Krýsa J. Pseudobrookite (Fe_2TiO_5) films: Synthesis, properties and photoelectrochemical characterization. *Catal. Today* **2023**, *413–415*, 113982.
39. International Centre for Diffraction Data. *Powder Diffraction File Alphabetic PDF-4 Data Base*; ICDD: Newtown Square, PA, USA, 2023.
40. Popkirov G, Schindler RM. Spectral dependence of the quantum efficiency of thin film semiconductor photoelectrodes. *Sol. Energy Mater.* **1986**, *13*, 161–174.